

A winter study case, comparing surface and vertical snowfall observations with the operational forecast model MEPS

Franziska Hellmuth



Thesis submitted for the degree of
Master in Meteorology
60 credits

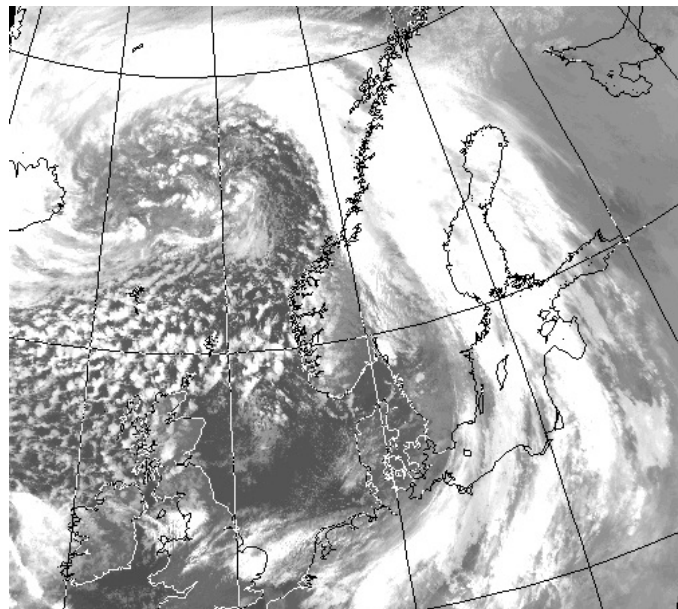
Department of Geoscience
Faculty of Mathematics and Natural Sciences

UNIVERSITY OF OSLO

Spring 2018

A winter study case, comparing surface and vertical snowfall observations with the operational forecast model MEPS

Franziska Hellmuth



Satellite image of the extreme extratropical cyclone on 24 December 2016 at the coast of Norway. Image obtained from the Dundee Satellite Receiving Station <http://www.sat.dundee.ac.uk>.

© 2018 Franziska Hellmuth

A winter study case, comparing surface and vertical snowfall observations with the operational forecast model MEPS

<http://www.duo.uio.no/>

Printed: Reprocentralen, University of Oslo

TABLE OF CONTENTS

LIST OF ABBREVIATIONS	III
CHAPTER 1: INTRODUCTION	1
CHAPTER 2: SITE, INSTRUMENTATION, DATA, AND METHODOLOGY	6
2.1 Haukeliseter site	6
2.2 Climate at Haukeliseter	8
2.3 Instruments	9
2.3.1 Double Fence Snow gauge	11
2.3.2 MRR - Micro Rain Radar	12
2.3.3 PIP - Precipitation Imaging Package	15
2.3.4 MASC - Multi-Angular Snowfall Camera	16
2.4 Optimal Estimation Retrieval Algorithm	16
2.4.1 Snowfall retrieval scheme	18
2.4.2 Environmental masks for the optimal estimation retrieval	23
2.5 MetCoOp Ensemble Prediction System	24
2.5.1 AROME - MetCoOP	25
2.5.2 Meso-NH and the ICE3 scheme	26
2.5.3 Adjustment of ICE3 inside MEPS	29
2.6 Numerical data transformation	29
2.6.1 Layer thickness in MEPS	29
2.6.2 Snow water content	30
2.6.3 Snow water path	31
2.6.4 Ensemble mean and Coefficient of Variation	31
2.6.5 Mean error and mean absolute error	32
2.6.6 Percent difference and average difference	32
CHAPTER 3: ANALYSIS OF THE CHRISTMAS STORM 2016	33
3.1 Extreme weather	34

3.2	Dynamic Tropopause map	34
3.3	Thickness, Sea Level Pressure, Total Precipitable Water, and wind at 250 hPa	37
3.4	Integrated Vapour Transport	37
3.5	Observations at the weather mast	40
3.6	Large scale circulation	40
CHAPTER 4: RESULTS AND DISCUSSION		49
4.1	Comparison of surface observations	49
4.2	Observation and predictions of large scale weather phenomena at the surface	53
4.3	Surface snowfall accumulation	62
4.4	Observation of large scale weather phenomena in the vertical	70
4.5	Orographic influence on precipitation	82
4.6	Discussion all	84
CHAPTER 5: SUMMARY AND CONCLUSION		89
REFERENCES		90
APPENDIX A: FORWARD MODEL		101
A.1	Scattering Model	101
APPENDIX B: RESULTS		104
B.1	48 h surface observations and MEPS forecasts	104
B.2	Mean error and mean absolute error	106
B.3	Hourly averages ensemble member zero and one	108
B.4	Vertical SWC - all ensemble member	110

CHAPTER 2: SITE, INSTRUMENTATION, DATA, AND METHODOLOGY

This chapter describes the site, instruments, the optimal estimation retrieval and the regional forecast model used to determine the vertical profile of snow water content for observed snow events. The determination of required parameters from the measuring instruments in relation to the optimal estimation retrieval will be explained. The purpose of this study is to compare the vertical observations from the Haukeliseter measurement site and the output from the operational forecast model at the Norwegian Meteorological Institute for the extreme weather event during Christmas 2016. The last section will give an insight on how the data was analysed to compare the different systems.

2.1 HAUKELISETER SITE

Haukeliseter, shown in Figure 2.1.1 is a mountain plateau 991 m above sea level, located in the Norwegian county 'Telemark' (59.8° N, 7.2° E, Figure 2.1.1). The station measures precipitation, temperature, snow depth and wind. It has served as a measurement site for snow accumulation since the winter of 2010/2011 [Wolff et al., 2010, 2013, 2015] and serves as WMO (World Meteorological Organization) station.

The study site is surrounded by mountain tops being 100 m to 500 m higher than the flat area. As seen in Figure 2.1.1c is Haukeliseter more open to the south and the south-west and the closest mountain top (situated to the NE) has an altitude of 1162 masl, [Wolff et al., 2015]. The mountains west to north exceed elevations of 1600 m.

A detailed setting of the measurement site is shown in Figure 2.3.1. The precipitation sensors are perpendicular to the predominant wind. Additional measurements of other

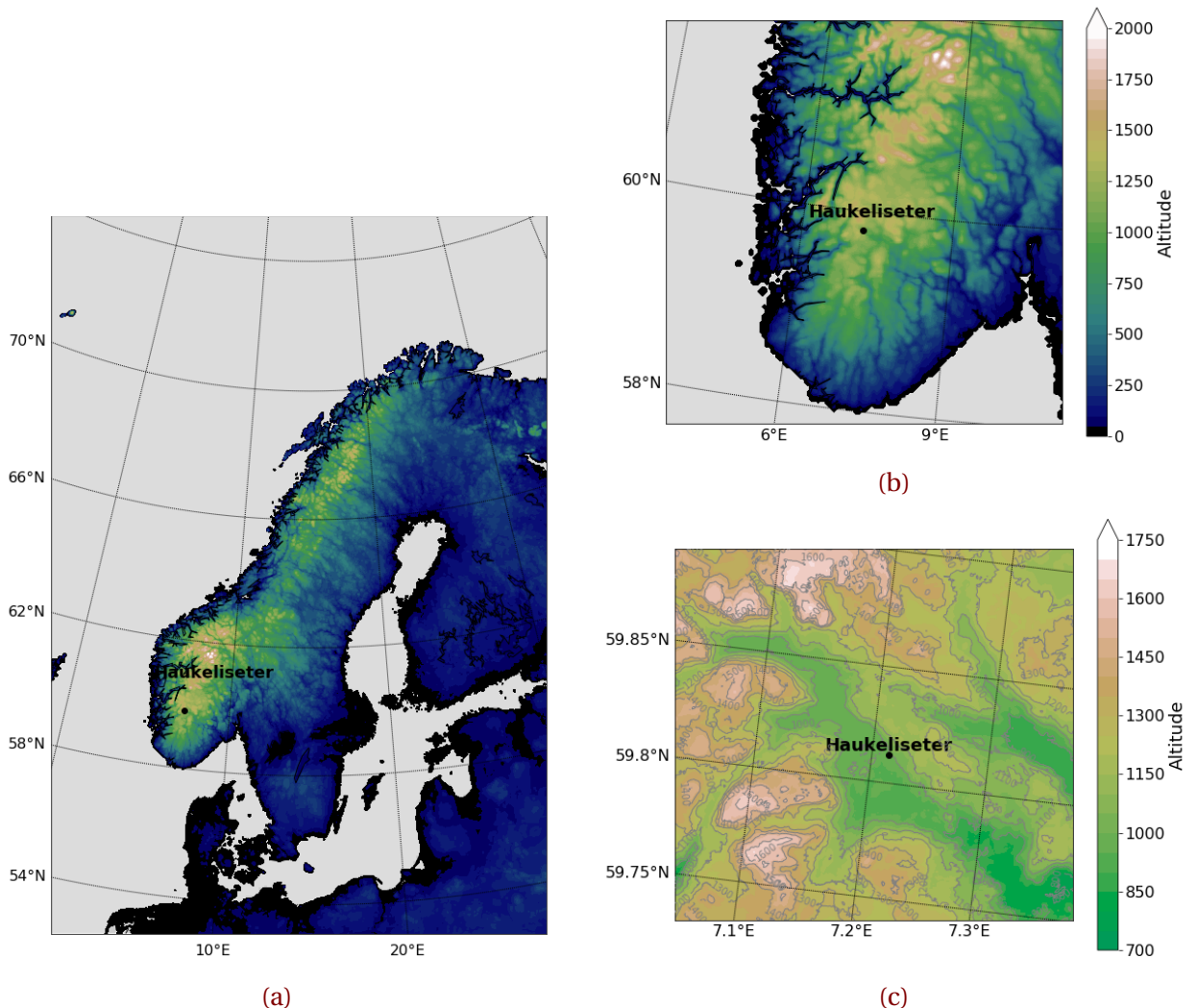


Figure 2.1.1: Model elevation map of Northern Europe (a) and Southern Norway (b), where the model domain of MEPS are presented in Lambert projection. The elevation corresponds to the legend of b. A topographic map of the measurement site is shown in c with DTM 10 Terrain Model (UTM33) from [Geonorge \[2018\]](#).

meteorological parameters such as temperature, wind, and pressure are used to connect the large-scale weather situation with the local measurements. The data is provided by [eklima \[2016\]](#), where the temperature is measured at double fence height. The hourly value of temperature is represented by the last minute value of the previous hour measurement. The 10 m wind is measured by an ultrasonic wind sensor from Gill, mounted at the tower

close to the double fence. Wind data is obtained from [eklima \[2016\]](#) and represents 10 min averages from the last 10 min of an hour.

2.2 CLIMATE AT HAUKELISETER

The general climate at Haukeliseter can be defined with the updated Köppen-Geiger climate types presented in [Peel et al. \[2007\]](#). Figure 8 in [Peel et al. \[2007\]](#) show, that Haukeliseter may lay in a transition zone and can be categorized as ET, a polar tundra climate type (hottest month temperature $T_{hot} \geq 0^{\circ}\text{C}$) or as Dfc, a cold climate without dry season and cold summers. Haukeliseter presents a typical Norwegian climate condition. At the measurement site, frequent snow events combined with high wind speeds are observed during a six to seven month winter period. In addition, a snow amount of about two to three meter can be expected, where 50 % of the yearly precipitation is solid in the form of snow, graupel or mixed-phase precipitation [[Wolff et al., 2010, 2013, 2015](#)].

The mean wind direction (Figure 2.3.1) for solid precipitation is from the west/east with maximum wind speed above 15 m s^{-1} , observed during a 10-year winter period at a nearby station [[Wolff et al., 2010, 2015](#)]. In Figure 2.2.1, the green dashed line represents the average December temperature of -6°C (30-yr period 1961 to 1990,[[eklima, 2016](#)]). December 2016 was warmer with an anomaly of +4.9 K above the climate mean. In 2016, the precipitation was 200 % more than the climate mean during December. This difference could be associated with the new installation of the double fence - Geonor gauge at Haukeliseter. In [Wolff et al. \[2015\]](#), Figure 5 shows that single fence precipitation gauges underestimate the amount of precipitation about 80 % during high wind speed events. Since the Double Fence construction was not in use before 2010/2011, which might have led to an observation of too little precipitation at Haukeliseter during winter and a followed incorrect climate statistic. The precipitation observed in the period of 21 to 27 December 2016 where 56.9 % of the total accumulated precipitation in December 2016. Furthermore, a maximum wind of 22.3 m s^{-1} was observed in this period, which can be associated with a slight storm (Section 3.5 and Table 3.5.1).

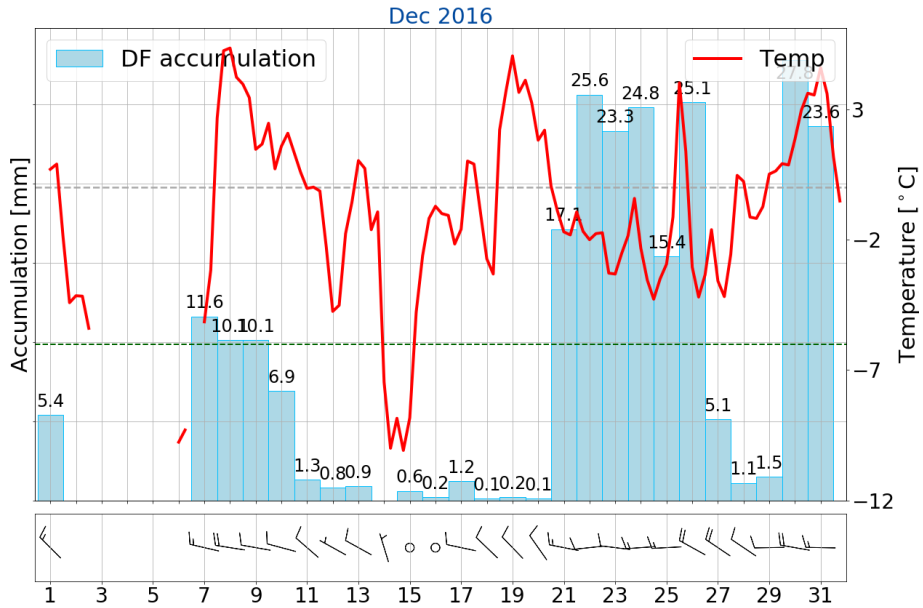


Figure 2.2.1: Observations at Haukeliseter weather mast during December 2016. The daily accumulation is presented in light blue [mm]; the six hour mean temperature in red, [°C], and daily maximum 10 m wind as barbs [m s^{-1}]. Gray dashed line indicates the freezing temperature. The freezing temperature is indicated by the green dashed line and the monthly normal value (-6.0°C) by the green [eklima \[2016\]](#). Note, no data was available from 2 to 6 December 2016.

2.3 INSTRUMENTS

The WMO site Haukeliseter, operated by Met-Norway serve numerous meteorological measurements of temperature, wind speed and direction. 10 m wind and 4.5 m air temperature are measured at the tower close to the double fence (Section 2.3.1). The wind measurements are performed with an ultrasonic wind sensor from Gill (Wind observer II with extended heating). Air temperature is obtained with a pt100 element at gauge height and protected by standard Norwegian radiation screen [Wolff et al., 2015]. Pressure?

Further information about the WMO site and the instrument setting, can be found in Wolff et al. [2013, 2015].

A collaboration between the University of Utah, University of Wisconsin and Met-Norway made it possible to install three additional instruments at the measurement site during winter 2016/2017. A Micro Rain Radar (MRR) is used to obtain particle reflectivity and Doppler velocity aloft, thus providing the vertical structure of the storm. Additionally, a

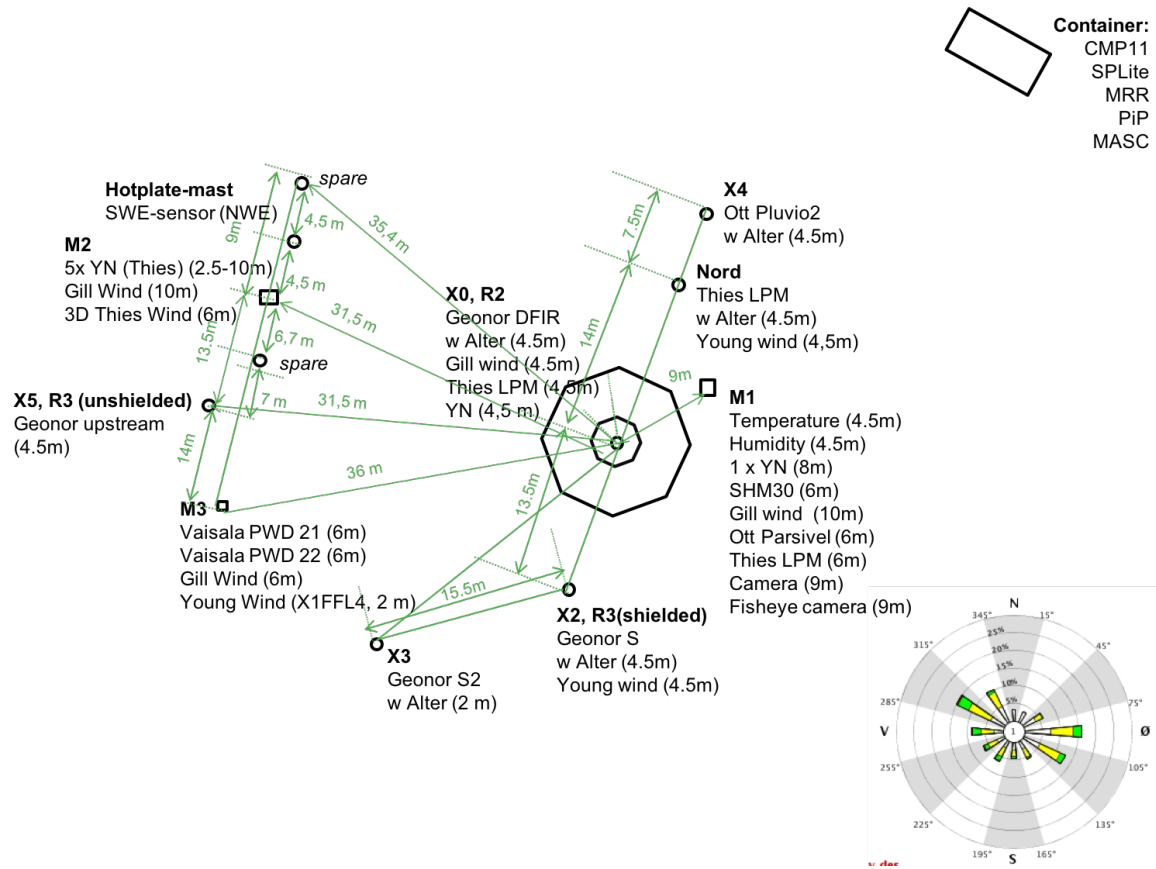


Figure 2.3.1: Instruments at the Haukeliseter measurement site during winter 2016/2017 [adapted from Wolff et al., 2015]. The windrose indicates the mean wind direction from either from west-north-west or east-south-east.

Multi-Angle Snowflake Camera (MASC) and a Precipitation Imaging Package (PIP) will be used to determine the snow habit, the snowfall particle size distribution, and the near-surface fall speed. Since many factors such as humidity and temperature contribute to snowflake geometry, the use of these instruments will provide knowledge of snowflake habits, particle size distributions, and fall speed crucial to reduce error in snowfall retrievals.

A sketch of the instrumentation setting is presented in Figure 2.3.1. The octagonal indicates the double fence. The container is north-east from the double fence having the MRR, MASC and PIP mounted at the top. **M1** in Figure 2.3.1 is the 10 m weather mast, providing

the hourly [eklima \[2016\]](#) temperature, pressure, and wind measurements. The mean wind direction from west-north west and east-south east are shown in the wind rose in Figure 2.3.1.

2.3.1 DOUBLE FENCE SNOW GAUGE

Since the winter 2010/2011 Haukeliseter is equipped with several precipitation gauges. The wind shielded gauges are placed perpendicular to the main wind direction (E/W wind).

The wind-induced under-catch of solid precipitation is determined by [Wolff et al. \[2015\]](#). The wind plays different roles in the amount of accumulation depending on the kind of precipitation. For temperatures below -2°C the wind speed influences the falling snow. Where less precipitation can be observed at higher wind speeds or more precipitation can be measured if too much is blown into the gauge. The catch ratio between the standard Geonor precipitation gauge and the Double Fence - Geonor (Figure 2.3.2a) shows that only 80 % of solid precipitation is observed at wind speeds of 2 m s^{-1} whereas only 40 % at 5 m s^{-1} , Figure 5 in [Wolff et al. \[2015\]](#).

The precipitation gauge protected by an octagonal double fence (Figure 2.3.2a) is more accurate than the single fence and will be used as the reference to all surface accumulation measurements. The double fence creates an artificial calm wind and maximize the catch of precipitation, [\[Wolff et al., 2010, 2013, 2015\]](#). The wind inside the double fence is measured to be not much higher than 5 m s^{-1} even if the winds out-

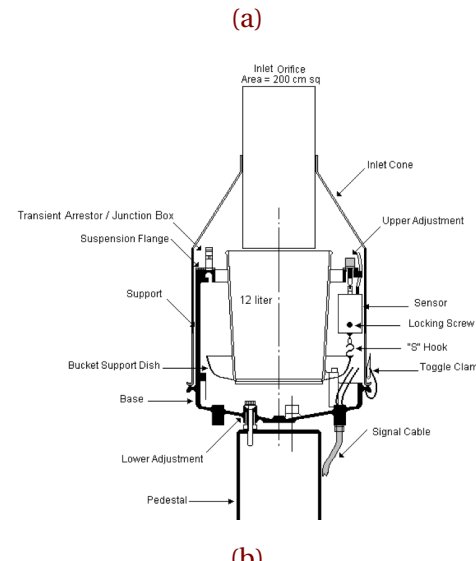


Figure 2.3.2: a: Double fence and unprotected precipitation gauges at Haukeliseter, from [Wolff et al. \[2015\]](#). The prevailing wind direction from east comes from the lower, left corner in the image and the west wind from the opposite site. b: Vertical cross section of T-200B precipitation gauge [[Geonor Inc., 2015](#)].

side exceed 20 m s^{-1} (occurred 26 December 2016).

This shows the need of a combination of ground-based observations together with an optimal estimation retrieval to verify the accuracy of MEPS. Wolff et al. [2015] introduced an adjustment function for the Geonor double fence, so that different precipitation under certain wind speeds are presented correctly and can be used as confidential data. For now, it is presumed that the average under catch inside a double fence is 20 % for wind speeds between 10 m s^{-1} and 20 m s^{-1} and 10 % for wind speeds below 9 m s^{-1} [Wolff, 2018].

Inside the double fence is a precipitation-weighing gauge Geonor T-200B3 [3-wire transducers, 1000 mm, Geonor Inc., 2015] with an Alter wind screen to reduce wind turbulence around the gauge. At Haukeliseter the orifice height of the Geonor is 4.5 m above the ground because of an expected snow depth of two to three meter during a winter season and the likelihood of measuring drifting snow [Wolff et al., 2013, 2015].

A vertical cross section of the T-200B gauge is shown in Figure 2.3.2b. The precipitation particles fall through the 200 cm^2 orifice protected with a heated collar, into a cylindric bucket filled with frost protection. The bucket is placed on top of a Bucket Support Dish [Figure 2.3.2b, Geonor Inc., 2015]. This dish is connected with three wire sensors having an eigenfrequency changing with the weight inside the bucket. A formula provided by Geonor Inc. [2015] calculates the amount of precipitation with the frequency of each sensor. The three sensors provide a reduction of an error in connection with an unlevel installation. Met-Norway average the values of all three sensors and provide hourly data at **eklima**.

2.3.2 MRR - MICRO RAIN RADAR

Radar are very useful to observe the vertical profile of the atmosphere. The instrument detects mesoscale features and makes it possible to visualise the vertical structure of storms [Markowski and Richardson, 2011].

The principle of radar measurements is based on an electromagnetic wave, which is emitted from the radar transmitter and interacts with the hydrometeors along the beam. A fraction of the



Figure 2.3.3: Micro Rain Radar at the measurement site in Kiruna.

pulse energy is reflected back to the receiver of the radar. The quantity of scattering depends on the shape and structure of the reflected particle. Vertical profiles of reflectivity give information about the diameter of the target object.

The Micro Rain Radar (Figure 2.3.3) measures profiles of Doppler spectra [METEK, 2010]. The Doppler spectrum describes the movement of the particle. The vertical pointing Doppler radar measures the returning energy from each interval and enables the detection of the Doppler spectrum [L'Ecuyer, 2017]. The MRR has a frequency of 24 GHz and a temporal and spatial resolution of 60 s and 100 m, respectively. The radar height range from 100 m (because of ground clutter) to 3.000 m [METEK, 2010].

MRR radar reflectivity (Z) is transformed from $1 \text{ mm}^6/\text{m}^3$ to dBZ, by the following relationship;

$$Ze = 10 \log_{10} \left(\frac{Z}{1 \text{ mm}^6/\text{m}^3} \right) \quad [\text{dBZ}] \quad (2.3.1)$$

A transformation to rainfall rates can be performed by the Z - R (reflectivity - rainfall) relationship. The rainfall rate in each layer can be estimated by the use of typical fall speeds and the Marshall-Palmer particle size distribution for liquid particles [Rinehart, 2010], Equation (2.3.2)

$$\begin{aligned} Z &= 200R^{\frac{8}{5}} \quad [\text{mm}^6\text{m}^{-3}] \\ R &= \left(\frac{10^{\frac{Ze}{10}}}{200} \right)^{\frac{5}{8}} \quad [\text{mmh}^{-1}] \end{aligned} \quad (2.3.2)$$

The Z-R relationship with the Marshall-Palmer assumption (Equation (2.3.2)) applied is represented in Table 2.3.1. Z-snowfall relationships are developed but are difficult to apply due to the variation of size and density of the particles [L'Ecuyer, 2017].

After the transformation to dBZ the reflectivity is averaged for every 200 m thick layers, where only values above 300 m taken into account, e.g. a reflectivity at 400 m represents the mean value of reflectivity between 300 m and 500 m.

Table 2.3.1: Typical reflectivity values, according to Doviak and Zrnic [1993], obtained from measurements, models, and observations. The rainfall rate R is calculated with Equation (2.3.2).

	Ze [dBZ]	R [mm h ⁻¹]
Drizzle	<25	1.3
Rain	25 to 60	1.3 to 205.0
Snow		
dry, low density	<35	5.6
Crystal; dry, high density	<25	1.3
wet, melting	<45	23.7
Graupel		
dry	40 to 50	11.5 to 48.6
wet	40 to 55	11.5 to 99.9
Hail		
small; <2 cm, wet	50 to 60	48.6 to 205.0
large; >2 cm, wet	55 to 70	99.9 to 864.7
Rain & Hail	50 to 70	48.6 to 864.7

2.3.3 PIP - PRECIPITATION IMAGING PACKAGE

The Precipitation Imaging Package (PIP) is a video disdrometer that is a modification of the Snowflake Video Imager presented by [Newman et al. \[2009\]](#). It consists of a halogen flood lamp and a video system that samples at 60 Hz (Figure 2.3.4). Both lamp and lens have a distance of approximately 3 m that follows a field of view: 32 mm by 24 mm.

In front of the halogen lamp there is a frosted window, so that the background light is uniform over all time. A falling particle appears as a 2-D shadow in the video image. Particle size distribution (PSD) and fall speed of precipitation can be determined from the black and white images provided by the system. The instrument also can give first order estimates of snowflake particle habit when in focus in the images. [Newman et al. \[2009\]](#) describes the details of the algorithm applied to the system to get information about the snow-particle habit. The winds have almost no effect on the result of the video distrometer [[Newman et al., 2009](#)]. To reduce eventual wind effects, the distrometer was oriented perpendicular to the mean wind.



Figure 2.3.4: Precipitation Imaging Package.

2.3.4 MASC - MULTI-ANGULAR SNOWFALL CAMERA

The Multi-Angular Snowfall Camera (MASC) takes high-resolution images of hydrometeors in free fall and measures the fall-speed simultaneously.

The MASC consists of three cameras, three flashes, and two near-infrared sensors, pointing at a ring centre (Figure 2.3.5). A hydrometeor has to pass through the ring in a certain way to trigger the near-infrared sensors. At the same time the three cameras take a picture of the falling particle. Since the cameras take pictures from three different angles, the particles size, shape, and orientation can be specified from an algorithm applied to the image, described in [Garrett et al. \[2012\]](#). Furthermore, the form and heritage of the hydrometeor, such as collision-coalescence, riming, capture nucleation, or aggregation, can be estimated.

The near-infrared sensor, that is used to trigger the cameras and the lights quantifies the fall-speed of the hydrometeors, by measuring the time the particle needs to pass the distance between the upper and lower trigger.

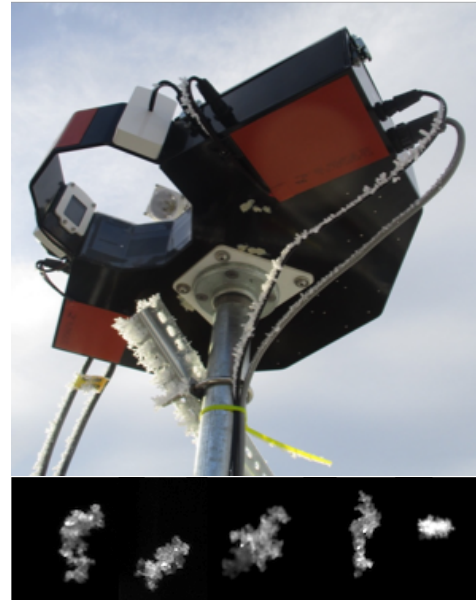


[Figure 2.3.5: MASC and images taken by instrument during the Christmas storm 2016.](#)

2.4 OPTIMAL ESTIMATION RETRIEVAL ALGORITHM

The quantitative estimation of snowfall at the global scale from spaceborne measurements has occurred only recently. Initial retrieval approaches were based on passive microwave measurements [[Noh et al., 2006](#), [Skofronick-Jackson et al., 2004](#)]. But since these passive measurements can only assess total integrated snow water path for a given column, such efforts were unable to provide much information on the vertical profiles of snow water. The launch of the CloudSat 94 GHz Cloud Profiling Radar (CPR) in 2006, however, provided the first opportunity to examine such vertical structure at a global scale. Several studies, such as [Matrosov \[2007\]](#) and [Kulie and Bennartz \[2009\]](#), have shown that the CPR

can be used to estimate snowfall rate but that estimated snowfall values depend heavily upon assumed snowflake microphysical properties. So, for a given radar reflectivity, we can get large differences in estimated snow rate depending upon retrieval assumptions such as snowflake habit and particle size distribution (PSD). For the operational CloudSat snowfall retrieval scheme (2C-SNOW-PROFILE), [Wood et al. \[2015\]](#) developed snowflake particle models based upon video snow disdrometer observations from the Canadian CloudSat-CALIPSO Validation Project [C3VP, [Hudak et al., 2006](#)]. Scattering properties for these snow particle models were based upon the Discrete Dipole Approximation (DDA) method. It was hoped that the use of realistic snow properties in the retrievals would lead to reasonable estimates of snowfall in the retrieval. In addition, they derived an a priori relationship between particle size distribution parameters and temperature that they could use as an additional constraint for the snowfall scheme. Use of the flexible optimal-estimation retrieval framework allowed a means to develop a best estimate of snow properties that are consistent with both the CPR reflectivities and the a priori constraint.

They have also been used to estimate snowfall in remote locations such as the Antarctic and Arctic [[Kulie et al., 2016](#), [Palerme et al., 2014](#)], that in turn, have been used to evaluate the representation of snowfall in climate models [[Christensen et al., 2016](#), [Palerme et al., 2017](#)]. Similarly, these estimates have been used to assess the performance of ground-based radar schemes such as those based upon the operational weather radar system in Sweden [[Norin et al., 2015](#)]. Despite such progress, however, the CloudSat scheme can still lead to uncertainties in the retrievals of up to 140 % to 200 % [[Wood, 2011](#)] for individual storms.

Again, these uncertainties arise from the large variance in snowflake microphysical properties as observed in nature. In response, [Cooper et al. \[2017\]](#) explored the use of in-situ, event specific observations of snowflake microphysical properties to improve radar-based retrievals of snowfall. This work was based upon observations from the Ka-band ARM Zenith Radar (KAZR) and Multi-Angle Snow Camera (MASC) deployed at the ARM Climate Facility Site at Barrow in Spring 2014. This ground-based 35 GHz retrieval scheme was modified from the space-borne 94 GHz CloudSat retrieval scheme developed by [Wood \[2011\]](#). But instead of using a temperature dependent a priori characterisation of PSD, [Cooper et al.](#) introduced the in-situ observations of particle size distribution through the a priori terms of the optimal-estimation framework.

Preliminary analyses suggest good performance for this retrieval scheme at Barrow. Estimates of snowfall from the [Cooper et al. \[2017\]](#) approach differed by 18 % relative to nearby National Weather Service snow gauge measurements for total accumulation over multiple snow events. However, given limited snowfall observed at Barrow during the MASC deployment, it was difficult to come to any definitive conclusions about retrieval performance. The NSF (National Science Foundation) funded field campaign with MRR, MASC, and PIP (Precipitation Imaging Package) deployment at Haukeliseter provides an ideal opportunity to further explore this retrieval approach. This study will continue to examine the sensitivity of retrieval surface snowfall rate to assumptions of habit, fall speed, and particle size distribution as in [Cooper et al. \[2017\]](#). But the work presented here will be different in that we also will examine the vertical profiles of snowfall through the atmospheric column.

2.4.1 SNOWFALL RETRIEVAL SCHEME

The optimal estimation snowfall retrieval tries to achieve an estimate about the snow water content in the atmosphere. Snow water content in the atmosphere can be found from vertical reflectivity profiles, temperature at the surface and the PIP and MASC measurements. The inversion approach that is going to be used in this study requires to do forward model fluctuations. The optimal estimation retrieval will invert the measured reflectivity to estimate SWC, hence trying to figure out what SWC in the atmosphere is causing these reflectivities. The difference between inverse model and forward model is schematically shown in Figure 2.4.1. Atmospheric properties are difficult to find by using observations, because unknown parameters influence the measurement.

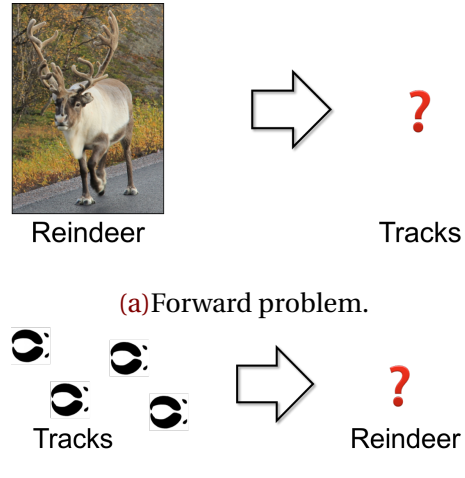


Figure 2.4.1: **a:** Relationship between parameter of interest (reindeer) and the unknown parameter of measurements (tracks). **b:** Inverse problem when the parameter of measurements is known but the parameter of interest is not [[Stephens, 1994](#)].

In principle, the forward model is a relationship between what can be measured and what one wants to know. This shows a relationship between the radar observations and the retrieved state vector \mathbf{x} . The received reflectivity is affected during the transmittance because of atmospheric effects. The received MRR reflectivity is presented by the reindeer in Figure 2.4.1a, and the unknown properties before attenuation are presented as tracks. The forward model will help to find simulated observations before the attenuation in the atmosphere took place and simulates the reindeers track. Since some aspects of the physical state of the reflectivity profiles are unknown, snow particle characteristics are possible to include into the system. This is called the inverse problem Figure 2.4.1b. It is how to determine what one wants to know given what can be measured. Let's say the track, or reflectivity profiles are known and a guess, a , about the SWC at Haukeliseter is made. The inverse problem tries then to solve for what would the MRR receive given this information? Hence the track is known, but the information of the reindeer is unknown (Figure 2.4.1b).

Optimal estimation is the balance between what the data can tell about the state and what is already known about it (MRR reflectivities; particle information from MASC, PIP; surface temperature). The optimal estimation method is based on Gaussian statistic, trying to minimize the scalar cost function, Φ for the snowfall properties, \mathbf{x} , the tracks in Figure 2.4.1b). The log-transformed values for the particle size distribution (PSD) slope parameter, λ , and N_0 the number intercept try to achieve the state vector \mathbf{x} of unknown microphysical properties.

$$\mathbf{x} = \begin{bmatrix} \log(\lambda)_0 \\ \vdots \\ \log(\lambda)_{\text{nlayer}} \\ \log(N_0)_0 \\ \vdots \\ \log(N_0)_{\text{nlayer}} \end{bmatrix} \quad \text{nlayer} = 14 \quad (2.4.1)$$

The retrieved PSD parameters, λ and N_0 , are dependent on the moist adiabatic lapse rate variation in each layer bin of the a priori temperature, T_{ap} . [Wood \[2011\]](#) showed a linear fit

between $\log(\lambda)$, $\log(N_0)$ and the changing a priori temperature. The following logarithmic assumption and T_{ap} in °C is used for each layer bin to achieve the state vector \mathbf{x} , to define the logarithmic slope parameter and number intercept.

$$\log(\lambda) = -0.03053 \cdot T_{ap} - 0.08258 \quad [\log(\text{mm}^{-1})] \quad (2.4.2)$$

$$\log(N_0) = -0.07193 \cdot T_{ap} + 2.665 \quad [\log(\text{m}^{-3} \text{mm}^{-1})] \quad (2.4.3)$$

The log-transformed equation is useful, since the results from C3VP were similar to other observations. The study showed, that N_0 ranges over several order of magnitude as well as λ was non-Gaussian for the snow events [Wood \[2011\]](#).

The cost function can be determined, knowing the retrieved particle size distribution parameters, which weights the difference between the observed reflectivity and the simulated measurements as well as the difference between the estimated and a priori guess.

$$n(r) = N_0 \exp(-\lambda r) \quad [\text{m}^{-3} \text{mm}^{-1}] \quad (2.4.4)$$

r is the particle maximum dimension evaluated from the 2D-scattering model for branched 6-arm spatial particles with porosities for reflectivity measurements at 24 GHz (see [Appendix A.1](#)).

Information about the retrieved state vector can then be used to minimize the scalar cost function:

$$\begin{aligned} \Phi(\mathbf{x}, y, a) = & (y - F(\mathbf{x}))^T \mathbf{S}_y^{-1} (y - F(\mathbf{x})) \\ & + (\mathbf{x} - a)^T \mathbf{S}_a^{-1} (\mathbf{x} - a) \end{aligned} \quad (2.4.5)$$

where, \mathbf{x} , vector of retrieved snowfall properties ([Equation \(2.4.1\)](#)); y , vector of observation (MRR reflectivity) ; a , vector of the a priori guess (temperature dependent); \mathbf{S}_a , a priori error covariance matrix; \mathbf{S}_y , measurement error covariance matrix. The forward model $F(\mathbf{x})$ presented in [??](#), relates unknown snowfall parameters \mathbf{x} to radar observations y and approximates the true physical state between them [[Cooper et al., 2017](#), [Wood et al., 2014](#)]. \mathbf{S}_a links the uncertainties of the PSD information and the surface temperature differences. The diagonal matrix elements in \mathbf{S}_a are equal to 0.133 and 0.95 for the particle slope parameter and the number intercept respectively as from Eq. 7.35 and 7.36 in [Wood \[2011\]](#).

\mathbf{S}_y characterises the uncertainties associated with the MRR measurements and calibration errors, as well as errors due to forward model assumptions. Wrong PSD, particle model assumptions or wrongly estimated fall speed are included as well in the \mathbf{S}_y error covariance. This study uses for the diagonal matrix elements 2.5² **based on the study from CITATION. BECAUSE.**

The retrieved state vector error covariance \mathbf{S}_x , estimates the error in the retrieved snow water content.

$$\mathbf{S}_x = \left(\mathbf{S}_a^{-1} + \mathbf{K}^T \mathbf{S}_y^{-1} \mathbf{K} \right)^{-1} \quad (2.4.6)$$

Equation (2.4.6) is the error related to the slope parameter, λ , and the number intercept, N_0 , which follows for \mathbf{x}

$$\mathbf{x} = \underbrace{\left(\mathbf{S}_a^{-1} + \mathbf{K}^T \mathbf{S}_y^{-1} \mathbf{K} \right)^{-1}}_{\mathbf{S}_x} \left(\mathbf{S}_a^{-1} \mathbf{a} + \mathbf{K}^T \mathbf{S}_y^{-1} (y - F(\mathbf{x}) + \mathbf{K}\mathbf{x}) \right) \quad (2.4.7)$$

The Jacobian matrix \mathbf{K} , describes how much the true state \mathbf{x} will change if the simulated values change and the sensitivity of the perturbed results. The closer \mathbf{K} is diagonal, the more is \mathbf{x} determined by the real observed and a priori values. If the limit of the partial derivative is close to unity, the retrieved value \mathbf{x} is its true state [Wood, 2011].

The retrieved values are tested for convergence in each retrieval cycle. If the cost function never gets close enough to the convergence criteria (= 2), then the estimated values are not matching the observations.

$$\hat{x} = (\mathbf{x} - F(\mathbf{x}))^T \mathbf{S}_x^{-1} (\mathbf{x} - F(\mathbf{x})) \quad (2.4.8)$$

Furthermore, a χ^2 test is performed at the convergence of \mathbf{S}_x to test the result of the retrieved state vector, \mathbf{x} .

$$\begin{aligned} \chi^2 &= (F(\mathbf{x}) - y)^T \mathbf{S}_y^{-1} (F(\mathbf{x}) - y) \\ &\quad + (\mathbf{x} - \mathbf{a})^T \mathbf{S}_a^{-1} (\mathbf{x} - \mathbf{a}). \end{aligned} \quad (2.4.9)$$

The first term in Equation (2.4.9) measures the part of χ^2 related to the noise of the forward model, and the second part quantifies the relation to the state vector. Thus, the second

term describes the accuracy of the quantities within the reflectivity and temperature measurements [Rodgers, 2000].

After the values of \mathbf{x} by Newtonian iteration [Eq. 5 Wood et al., 2014] are found, the snow water content in each layer is estimated from the knowledge of the snow particle mass-dimension relationship in Appendix A.1, and a PSD related to slope parameter and number intercept (Equations (2.4.2–4)).

$$\text{SWC} = \int_{r_{min}}^{r_{max}} m(r)n(r)dr \quad [\text{gm}^{-3}] \quad (2.4.10)$$

Attenuation in the atmosphere needs to be account for, to achieve a relationship between the reflectivity and the snowfall amount, which is small for frozen particles at a frequency of 24 GHz. The reflectivity for Rayleigh approximated, singly-scattered non-attenuated ice particles can be estimated, by using the previously calculated PSD (Equation (2.4.4)) and backscattering cross-section σ_{bk} [Kulie and Bennartz, 2009, L'Ecuyer and Stephens, 2002, Wood et al., 2015]. The Rayleigh approximation assumes, that $2\pi r/\lambda \ll 1$, where λ the wavelength of incident radiation.

$$\begin{aligned} \eta_{bk} &= \int_{r_{min}}^{r_{max}} n(r)\sigma_{bk}dr \quad [\text{m}^{-1}] \\ Ze^{ss,na} &= \frac{\Lambda^4}{\|K_w\|^2 \pi^5} \eta_{bk} \quad [\text{mm}^6 \text{m}^{-3}] \end{aligned} \quad (2.4.11)$$

where, Λ is the wavelength of the radar; $\|K_w\|^2$ is the complex refractive index of water and varies between 0.91 and 0.93 for wavelength between 0.01 m and 0.10 m and is independent of temperature. A complex refractive index for ice $\|K_i\|^2$ also exists, which is 0.18. This is valid for a density of 0.917 gcm^{-3} and independent of temperature and wavelength in the microwave region [Doviak and Zrnic, 1993]. In this work, $\|K_w\|^2 = 0.93$ is chosen.

Why did we choose K_w and not the one for ice?

The snow water content (Equation (2.4.10)) has to be transformed, to achieve snowfall water rates at the surface. An assumed climatological particle fall speed average of $V = 0.85 \text{ ms}^{-1}$ and the retrieved SWC (Equation (2.4.10)) gives the snow mass flux $J_{snow} = \text{SWC} \cdot V$ in $[\text{kgm}^{-2} \text{s}^{-1}]$. The precipitation amount at the surface is calculated, to compare retrieved snowfall rates to double fence measurements and the forecast model

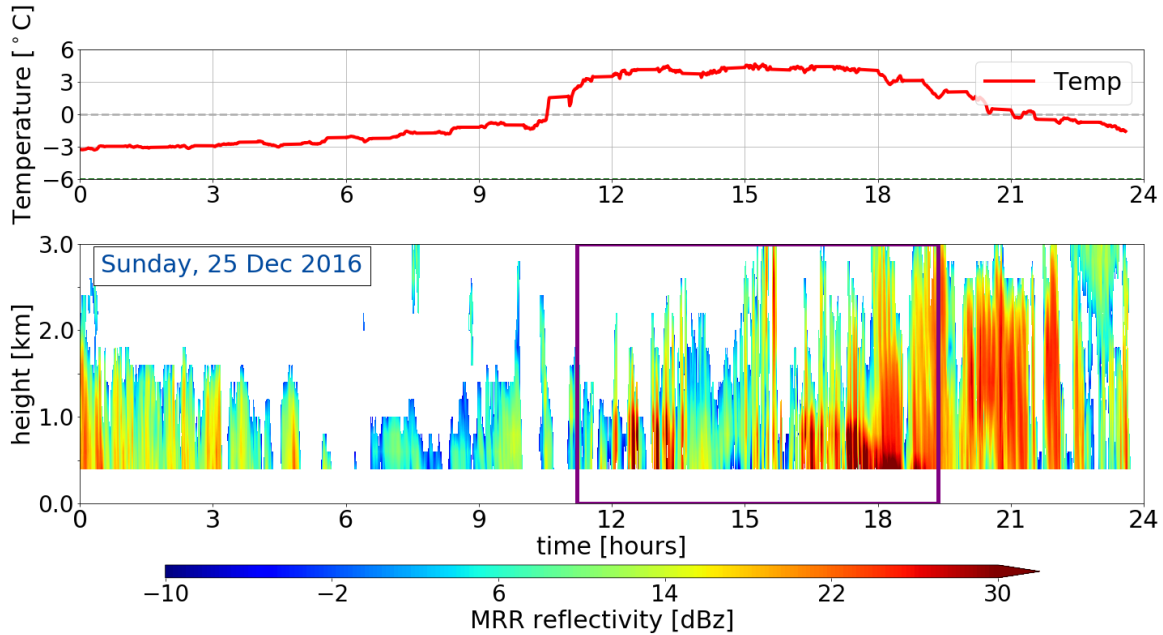


Figure 2.4.2: A priori temperature dependence within the optimal estimation retrieval for an all day precipitation event on 25 December 2016. The upper panel shows the surface a priori guess, T_{ap} , measured at the Haukeliseter site. The lower panel presents the reflectivity measure by the MRR. Additionally, indicates the purple frame the time, where the MRR reflectivity was larger than -10 dBZ and surface temperatures less than 2°C

output.

$$P = J_{snow} \times 10^{-3} \cdot (3600 \text{ s} \cdot 24) \quad [\text{mm d}^{-1}] \quad (2.4.12)$$

The precipitation amount at the surface, are taken to be equal to the values at the snow layer in 400 m, the lowest level of the obtained averaged MRR reflectivity (presented in Chapter 4).

2.4.2 ENVIRONMENTAL MASKS FOR THE OPTIMAL ESTIMATION RETRIEVAL

Different steps and assumptions are done in the here presented snowfall retrieval, to achieve vertical profiles of snowfall from MRR. The snowfall rate at the surface can be estimated from one of the lower levels. The optimal estimation retrieval is only performed for profiles, which are likely to have observed snow, where most retrievals use rain. Relationships between reflectivity and snowfall have been developed in previous studies. Different

crystal shapes led to different results, even if the PSD of ice particles is known. Snow densities vary significantly from storm to storm, where small particles are still Rayleigh scattered, and larger particles non-Rayleigh scattered [Gunn and East, 1954].

A reflectivity threshold of -15 dBZ is used, to obtain the likelihood of present snow. The threshold is similar to the one used in Wood et al. [2013]. Light liquid precipitation is related to -10 dBZ [Stephens and Wood, 2007]. Wood [2011] found, that the reflectivity above -15 dBZ are not influenced by ground clutter, when the reflectivity in the lowest bin and adjacent bin is compared.

The Haukeliseter measurement site is equipped with a weather mast, measuring the air temperature every minute at two-meter height (compare Figure 2.4.2, upper panel). Since the MRR measures above 300 m and temperature measurements exists only at the surface, a priori temperature (T_{ap}) is assumed to be similar to the observed near-surface air temperature. The use of a moist adiabatic lapse rate of $dT/dz = 5 \text{ K km}^{-1}$ gives T_{ap} in each layer. Snow existence at temperature measurements up to a threshold of $2 \text{ }^{\circ}\text{C}$ are assumed. Liu G. [2008] validated this threshold, by analysing present weather reports to find the distinction between liquid and solid precipitation.

The purple line in the lower panel of Figure 2.4.2 represents the time frame during 25 December 2016, where the MRR reflectivity is less than -15 dBZ , and a priori temperature passes the $2 \text{ }^{\circ}\text{C}$ limit at the surface.

2.5 METCOOP ENSEMBLE PREDICTION SYSTEM

MEPS (MetCoOp Ensemble Prediction System) was newly operational at Met-Norway when the extreme weather occurred in Norway. Comparing model data with actual observations helps to verify the agreement between model prediction and ground-based measurements.

AROME-MetCoOp was operational from March 2014 until November 2016, when it was replaced with an ensemble prediction system (EPS) based on AROME-MetCoOp. MEPS is used as weather forecast at the Norwegian Meteorological Institute, the Swedish Meteorological and Hydrological Institute (SMHI) and the Finnish Meteorological Institute (FMI), [Køltzow, 2017, Müller et al., 2017].

2.5.1 AROME - METCoOP

In principle, MEPS is a short-term weather forecast consisting of a ten ensemble member forecast system with 66 h prediction time and a horizontal resolution of 2.5 km and 65 vertical levels. One of the members is the deterministic forecast where the other nine present the perturbed state of the deterministic forecast. The initialisation of each member is performed at 0 UTC, 6 UTC, 12 UTC and 18 UTC [MetCoOp Wiki, 2017].

Forecast data saved for the deterministic and first ensemble member have a time resolution of one hour for 66 h. The other eight members have values every three hours for up to 48 h forecast time.

Figure 2.1.1a shows the MEPS model domain and its elevation as it was operational for December 2016. It covers the Nordic Countries including open water such as the Atlantic Ocean, the North and the Baltic Sea. A representation of the horizontal resolution zoomed on the Haukeliseter site is shown in Figure 2.5.1. Haukeliseter is surrounded by a complex terrain with mountains up to 1500 m to the west and the north and the more open terrain to the south-east.

The centre of the model is approximately at 63.5° N, 15° E. The horizontal grid points are projected on a Lambert projection to receive the same area size of each grid cell. The outer, parent grid is the ECMWF-IFS model (European Centre for Medium-Range Weather Forecasts Integrated Forecasting System) with a horizontal resolution of 9 km [Homleid and Tveter, 2016]. The ECMWF-IFS forecasts are used 6 h prior to the actual cycle in MEPS. Vertical hybrid coordinates are terrain-following and are mass-based, [Müller et al., 2017]. How the vertical hybrid coordinates are transformed into layer thickness or height is described in Section 2.6.1. Furthermore, MEPS underlies non-hydrostatic dynamics, MetCoOp Wiki [2017].

The representation of snow is covered by a modification of the three-class ice parametriz-

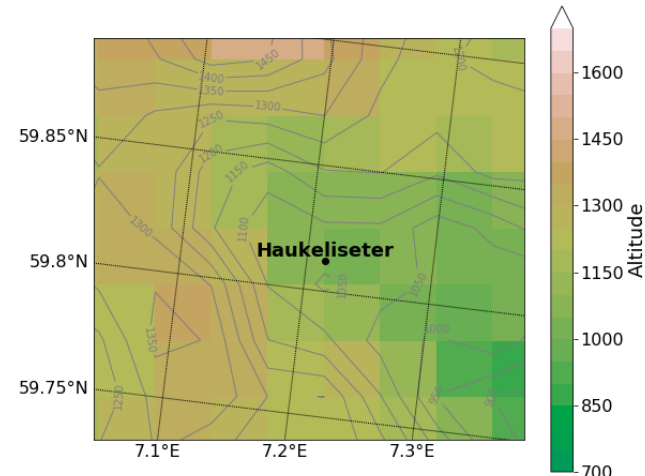


Figure 2.5.1: Representation of the topography around measurement site Haukeliseter in MEPS. Contours and shading present the elevation of the grid cells.

The horizontal grid points are projected on a Lambert projection to receive the same area size of each grid cell. The outer, parent grid is the ECMWF-IFS model (European Centre for Medium-Range Weather Forecasts Integrated Forecasting System) with a horizontal resolution of 9 km [Homleid and Tveter, 2016]. The ECMWF-IFS forecasts are used 6 h prior to the actual cycle in MEPS. Vertical hybrid coordinates are terrain-following and are mass-based, [Müller et al., 2017]. How the vertical hybrid coordinates are transformed into layer thickness or height is described in Section 2.6.1. Furthermore, MEPS underlies non-hydrostatic dynamics, MetCoOp Wiki [2017].

ation (ICE3) scheme. Where liquid-phase processes are separated from slow ice-phase processes and described in Section 2.5.2. To model the snow cover an one-layer atmosphere model scheme is implemented. This includes three variables such as: snow water equivalent (SWE), snow density, and snow albedo [Müller et al., 2017].

As synoptic observations are included in the model the snow-depth predictions underlay a special performance. Observations of snow-depth are only available at 6 UTC and 18 UTC, therefore is the snow analysis only performed twice daily [Homleid and Tveten, 2016, Müller et al., 2017].

2.5.2 MESO-NH AND THE ICE3 SCHEME

The physical parametrization within AROME is based on the French research communities' mesoscale non-hydrostatic atmosphere model (Meso-NH). The microphysical scheme in the Meso-NH atmospheric simulation system is based on the ICE3 scheme. The purpose of the scheme is to model as correctly as possible the ice phase in the atmosphere [Pinty and Jabouille, 1998]. McCumber et al. [1991] concluded from their case study, that at least three different ice categories are necessary to cover most precipitation but that applications might be case specific. According to the Meteo France [2009] documentation, the ice phase microphysical scheme must include:

\mathbf{r}_i : pristine ice phase

\mathbf{r}_s : snowflake type from lightly rimed large ice crystals or dry clusters, and

\mathbf{r}_g : heavily rimed crystals, such as graupel, frozen drops or hail

Within the ICE3 scheme no distinction between hail and graupel exists and therefore is the physical discrimination in the growth mode of graupel and hail is neglected.

To achieve snow water content within MEPS the total number concentration, slope parameter, mass diameter and the particle size distribution have to be determined. According to Caniaux et al. [1994] follows the particle size distribution the Marshall-Palmer distribution similar to Equation (2.4.4). The goal is to use a varying number concentration N_0 dependent on the ice category. The study has shown that N_0 can be assumed with

$$N_0 = C\lambda^x \quad (2.5.1)$$

$$\log_{10} C = -3.55x + 3.89$$

where C and x depend on the ice category and represent the relation between each other in Equation (2.5.1).

The ice water content for primary ice, snowflakes and rimed crystals is then assumed to be similar to Equation (2.4.10), but the integration limits range from zero to infinity and mass, and particle size distribution are dependent on the diameter of the particle. The mass diameter and particle size distribution (Equations (2.5.2) and (2.5.3)) are represented depending on the ice category shown in Table 2.5.1

$$m(D) = aD^b \quad (2.5.2)$$

$$n(D) = N_0 g(D) \quad (2.5.3)$$

and $g(D)$ to be the generalised Gamma function

$$g(D) = \frac{\alpha}{\Gamma(\nu)} \lambda^{\alpha\nu} D^{\alpha\nu-1} \exp(-(\lambda D)^\alpha) \quad (2.5.4)$$

with α , ν the shape and tail dispersion parameters and $\Gamma(\nu)$ the gamma function.

After following the above equations including Equation (2.4.10) the slope parameter λ can be generated with $G(B)$ the gamma function.

$$\lambda = \left(\frac{\text{SWC}}{aCG(b)} \right)^{\frac{1}{x-b}} \quad (2.5.5)$$

Table 2.5.1: Characterization parameters from primary ice (r_i), snowflakes (r_s) and rimed crystals (r_g). Values are based on the references in [Meteo France \[2009\]](#) and in [Pinty and Jabouille \[1998\]](#).

	r_i	r_s	r_g
α, ν	3.3	1.1	1.1
a	0.82	0.02	196
b	2.5	1.9	2.8
c	800	5.1	124
d	1.0	0.27	0.66
C		5	5×10^5
x		1	-0.5

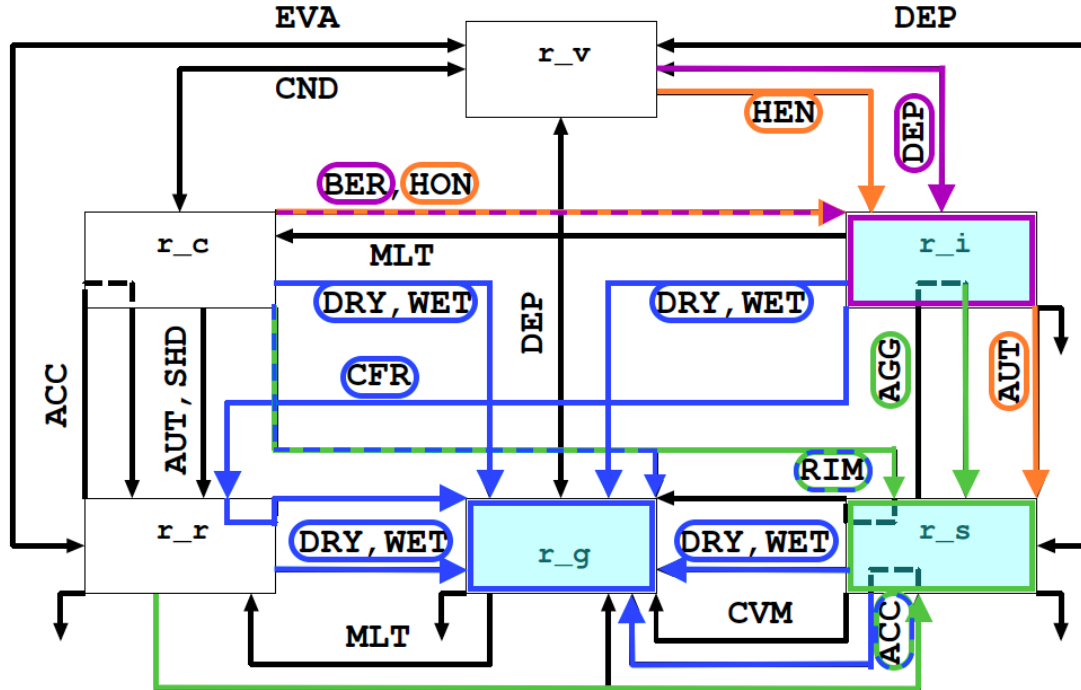


Figure 2.5.2: Microphysical processes for mixed phase clouds in the ICE3 scheme adapted from Meteo France [2009]. In orange the initiation processes for primary ice r_i and snowflakes r_s . The growing processes of r_i is shown in purple and for r_s in green. Graupel particles, r_g , grow from existent particles and the processes are shown in blue.

Meteo France [2009] documentation suggests starting the microphysics in the ICE3 scheme with 'slow' processes such as homogeneous and heterogeneous nucleation (HON, HEN), vapour deposition of snow and graupel particles (DEP), aggregation (AGG) and auto conversion (AUT), for ice processes right side in Figure 2.5.2. The second step is to initiate the warm processes left side in Figure 2.5.2. Then include the aggregation and conversion-melting (CVM) for snowflakes and contact freezing of raindrops (CFR). Add AGG and melting for graupel (MLT), and then the melting from pristine ice and the Wegener-Bergeron-Findeisen (BER) effect and lastly the sedimentation terms.

Figure 2.5.2 shows the summary of the microphysical processes for mixed phase clouds. The study focuses mostly on solid precipitation particles and therefore only the initiation and growth of pristine ice crystals r_i , snowflakes r_s , and rimed crystals r_g is presented. Following Pinty and Jabouille [1998] and Figure 2.5.2 it can be seen how AROME per-

forms the ice production. Orange lines in Figure 2.5.2 show the initiation of pristine ice crystals and snowflakes. In purple the growth mechanisms of r_i (BER,DEP). Green lines demonstrate the expansion of the snowflakes (RIM, AGG, ACC). Graupel (r_g) forms as an effect of heavy riming (RIM), by collision of larger raindrops with snowflakes (ACC), by WET/DRY growth or by contact freezing of raindrops (CFR). All graupel growth processes are indicated by blue lines in Figure 2.5.2, were hail formation is included.

2.5.3 ADJUSTMENT OF ICE3 INSIDE MEPS

Since the ICE3 scheme showed some weaknesses for the winter month, Müller et al. [2017] introduced some modifications. During cold conditions the ICE3-scheme showed too low temperature at two meter, too much ice fog and all year long was the occurrence of cirrus overestimated. After implementing the modifications described in Müller et al. [2017] the two meter temperature bias was reduced as well as an improvement of low-level clouds was shown. A negative aspect of these adjustments was that the occurrence of fog increased.

2.6 NUMERICAL DATA TRANSFORMATION

The following section will describe how the different variables where processed to achieve a comparison between the retrieved values and the forecast model output.

2.6.1 LAYER THICKNESS IN MEPS

To compare the measurements from the surface with the MEPS data, the closest grid point to Haukeliseter, is used.

MEPS has a vertical resolution in hybrid sigma pressure coordinates, were one is at the surface and decreases with height. To calculate the actual vertical pressure in Pa, a formula is provided in the OPeNDAP Dataset of `meps_full_2_5km_*.nc` by the Norwegian Meteorological Institute [2016].

$$p(n, k, j, i) = a_p(k) + b(k) \cdot p_s(n, j, i) \quad [\text{Pa}]. \quad (2.6.1)$$

p_s is the surface air pressure in Pa, and information about the variables a_p , b are not given from the access form. [Find reference for sigma-hybrid coordinate transformation](#)

equation.

The next step was to convert pressure-levels into actual heights by the use of the hypsometric equation. Here, the air temperature in model levels is used to calculate the mean temperature of each layer.

$$\bar{T} = \frac{\int_{p_1}^{p_2} T \partial \ln p}{\int_{p_1}^{p_2} \partial \ln p} \quad [\text{K}] \quad (2.6.2)$$

For the numerical integration, the Simpson rule was used, which is a build-in function in Python.

[Martin \[2006\]](#) presents steps of differentiating the hypsometric equation by using the virtual air temperature. But when the atmospheric mixing ratio is large, will the virtual temperature only be 1 % larger than the actual air temperature. Since the error is little calculations are done with the provided air temperature in model levels.

The thickness, Δz , of each layer is then be found by using the hypsometric equation from [Martin \[2006\]](#) and the previously calculated mean temperature (Equation (2.6.2)):

$$\Delta z = z_2 - z_1 = \frac{R_d \bar{T}}{g} \ln \left(\frac{p_1}{p_2} \right) \quad [\text{m}] \quad (2.6.3)$$

where R_d is gas constant for dry air with a value of $287 \text{ J kg}^{-1} \text{ K}^{-1}$, standard gravity $g = 9.81 \text{ m s}^{-2}$. p_1 and p_2 are the pressure levels at lower and higher levels, respectively ($p_2 < p_1$). To gain the respective height of each pressure layer, Δz is summed.

2.6.2 SNOW WATER CONTENT

To get a valid comparison between the SWC from the optimal estimation retrieval and the results from MEPS, the SWC is averaged over each hour. Taking the model initialisation of MEPS at 0 UTC the model produces forecast values at 0, 1, 2, ..., 22, 23, ..., 66 UTC. To approach hourly mean values from the retrieval SWC an average over 30 min prior and 29 min after each full hour is performed. This leads to a match of the average value at the same time as from MEPS.

Since MEPS has a higher vertical resolution than the optimal estimation snowfall retrieval each vertical profile of SWC is averaged every 200 m. To accomplish the same vertical

resolution only values above 100 m are used to start at the same range height as given from the MRR (Section 2.3.2).

Within the output from MEPS snow water content does not exist for each model layer. Hence the calculation of the SWC is performed by using the three solid precipitation categories given in MEPS. Namely the instantaneous mixing ratio of snowfall (r_s), graupel fall (r_g) and the atmosphere cloud ice content (r_i). The mixing ratios are represented in kg kg^{-1} and a transformation to gm^{-3} is performed. Densities in each model level (ρ_{ml}) are calculated and then multiplied with the sum of the solid precipitation mixing ratio.

$$\rho_{ml} = \frac{p_{ml}}{R_d T} \quad [\text{kgm}^{-3}] \quad (2.6.4)$$

$$\text{SWC}_{ml} = \rho_{ml} \cdot (r_s + r_g + r_i)_{ml} \cdot 10^6 \quad [\text{gm}^{-3}]. \quad (2.6.5)$$

2.6.3 SNOW WATER PATH

The snow water path (SWP) is the vertically integrated value of the averaged SWC (Equations (2.4.10) and (2.6.5)), where the numerical Simpson's integration is applied.

$$\int_{h_0}^{h_1=3000\text{m}} \text{SWC}(h) dh \approx \frac{h_1 - h_0}{6} \left[\text{SWC}(h_0) + \text{SWC}(h_1) + 4\text{SWC}\left(\frac{h_0 + h_1}{2}\right) \right] \quad [\text{gm}^{-2}] \quad (2.6.6)$$

The snow water path is a measure of the weight of ice particles per unit area. It indicates the total amount of ice in the atmosphere.

2.6.4 ENSEMBLE MEAN AND COEFFICIENT OF VARIATION

Check literature of meaning

The ensemble mean is the average of all ten ensemble members of MEPS.

$$\bar{x} = \frac{\sum_{i=1}^n x_i}{N} \quad (2.6.7)$$

The coefficient of variation is known as the standard deviation with respect to their mean of the model output. That means it shows the variation around the center or control run.

The standard deviation is defined as:

$$\sigma = \sqrt{\frac{\sum_{i=1}^n (x_i - \bar{x})^2}{N-1}} \quad (2.6.8)$$

which follows for the coefficient of variation:

$$CV = \frac{\sigma}{\bar{x}} \quad (2.6.9)$$

2.6.5 MEAN ERROR AND MEAN ABSOLUTE ERROR

The mean error for each ensemble member is calculated with:

$$ME = \frac{\sum_{i=1}^n MEPS_{ens} - DoFe_{obs}}{N} \quad (2.6.10)$$

where $MEPS_{ens}$ represents the value of each ensemble member and $DoFe_{obs}$ defines the observation from the double fence. For the mean absolute error follows then:

$$MAE = \frac{\sum_{i=1}^n |MEPS_{ens} - DoFe_{obs}|}{N} \quad (2.6.11)$$

2.6.6 PERCENT DIFFERENCE AND AVERAGE DIFFERENCE

The percentage difference presented in the results (Table 4.1.1 and add for MEPS) are calculated by:

$$\% \text{Difference} = \frac{SF - DoFe_{obs}}{DoFe_{obs}} \times 100 \quad (2.6.12)$$

SF presents the snowfall from the retrieval or the MEPS ensemble forecast. The average is then taken from all % Difference values to see the difference of the Christmas storm 2016.